Pairwise Comparison of [89]Zr- and [124]I-labeled cG250 Based on Positron Emission Tomography Imaging and Non-Linear Immunokinetic Modeling: *In Vivo* Carbonic Anhydrase IX Receptor Binding and Internalization in Mouse Xenografts of Clear Cell Renal Carcinoma

Sarah M. Cheal[1], **Blesida Punzalan**[1], **Michael G. Doran**[1], **Michael J. Evans**[2], **Joseph R. Osborne**[1], **Jason S. Lewis**[1,3,4], **Pat Zanzonico**[1,5], and **Steven M. Larson**[1,3,5]

[1]Department of Radiology, Memorial Sloan-Kettering Cancer Center, New York, New York

[2]Human Oncology and Pathogenesis Program, Memorial Sloan-Kettering Cancer Center, New York, New York

[3]Program in Molecular Pharmacology and Chemistry, Memorial Sloan-Kettering Cancer Center, New York, New York

[4]Radiochemistry and Imaging Sciences Service, Memorial Sloan-Kettering Cancer Center, New York, New York

[5]Molecular Pharmacology and Therapy Service, Memorial Sloan-Kettering Cancer Center, New York, New York

Abstract

Purpose—The positron-emitting tomography (PET) tracer, [124]I-cG250, directed against carbonic anhydrase IX (CAIX) shows promise for pre-surgical diagnosis of clear renal cell carcinoma (cRCC) [1, 2]. The radiometal zirconium-89 ([89]Zr), however, may offer advantages as a surrogate PET nuclide over [124]I in terms of greater tumor uptake and retention [3]. In the current report, we have developed a non-linear immunokinetic model to facilitate a quantitative comparison of absolute uptake and antibody turnover between [124]I-cG250 and [89]Zr- cG250 using a human cRCC xenograft tumor model in mice. We believe that his unique model better relates quantitative imaging data to the salient biologic features of tumor antibody-antigen binding and turnover.

Methods—We conducted experiments with [89]Zr-cG250 and [124]I-cG250 using a human ccRCC cell line (SK-RC-38) to characterize the binding affinity and internalization kinetics of the two tracers *in vitro*. Serial-PET imaging was performed in mice bearing sub-cutaneous cRCC tumors to simultaneously detect and quantify time-dependent tumor uptake *in vivo*. Using the known specific activities of the two tracers, the equilibrium rates of antibody internalization and turnover in the tumor were derived from the PET images using non-linear compartmental modeling.

For correspondence or reprints contact: Pat Zanzonico, 415 E. 68th Street, New York, NY 10065, Memorial-Sloan Kettering Cancer Center, 1275 York Ave, New York, NY 10021, Tel.: +1 212 888 2134 Fax +1 212 717 3263, zanzonip@mskcc.org.

Results—The two tracers demonstrate virtually identical tumor-cell binding and internalization but with markedly different retentions *in vitro*. Superior PET images were obtained using [89]Zr-cG250, owing to the more prolonged trapping of the radiolabel in the tumor and simultaneous wash-out from normal tissues. Estimates of cG250-CAIX complex turnover were $1.35–5.51 \times 10^{12}$ molecules per hour per gram of tumor (20% of receptors internalized per hour), and the ratio of [124]I/[89]Zr atoms released per unit time by tumor was 17.5.

Conclusions—Pairwise evaluation of [89]Zr-cG250 and [124]I-cG250 provided the basis for a non-linear immunokinetic model which yielded quantitative information about the binding and internalization of radioantibody bound to CAIX on tumor cells *in vivo*. [89]Zr-cG250 is likely to provide high-quality PET images and may be a useful tool to quantify CAIX/cG250 receptor turnover and cG250-accessible antigen density non-invasively in man.

Keywords

G250; ImmunoPET; Zirconium-89; Iodine-124; Non-Linear Kinetic Model

INTRODUCTION

The chimeric monoclonal antibody cG250 described by Oosterwijk and colleagues targets CAIX-- a transmembrane protein involved in control of interstitial pH in normal human tissues and tumors [4]. The antigen itself is under the regulatory control of hypoxia-inducible factor alpha (HIFα) and is upregulated uniformly in cRCC due to loss of the Von Hippel-Lindau (VHL) tumor suppressor.

The cG250 antibody has been used as a targeting vector for diagnostic and therapeutic radionuclides for management of advanced cRCC [1]. For example, diagnostic PET imaging with [124]I-cG250 has been reported to allow measurement of disease burden and distinguish clear-cell cancer from other histologies. Non-invasive staging is especially important in older patients with impaired renal function for whom surgery or even biopsy might be hazardous [5]. Also, Stillebroer et al. recently conducted a phase 1 radioimmunotherapy (RIT) study with ^{177}Lu-cG250 in patients with progressive metastasic cRCC, showing 17 of 23 (74%) having stable disease 3 months following treatment and one patient showing a partial response that lasted for 9 months [6].

Rational design of antibody-targeted tracers and drugs (such as cG250 conjugates) requires an understanding of the spatiotemporal disposition of the antibody in vivo and the inherently variable fate of the antibody-conjugated cargo (e.g. [124]I or ^{177}Lu). One must understand the kinetics of the binding and cellular processing of the antibody conjugate as well as of associated degradation products. For example, after the [124]I-cG250/CAIX complex is internalized *via* endocytosis, [124]I-iodotyrosine is rapidly expelled from the cell after lysosomal degradation [7]. Conversely, "residualizing" radiometals such as ^{111}In and ^{177}Lu are retained by the cell in the form of low-molecular weight catabolites [8]. This phenomenon has been demonstrated to have clinical consequences for cG250/CAIX imaging; for example, Brouwers, *et al.* performed a direct intra-patient comparison of single-photon emission computed tomography imaging of ^{131}I-cG250 and ^{111}In-cG250 in RCC metastases and found that the total number of lesions revealed was greater with

the ^{111}In-labeled tracer, due to the higher activity overall in the lesions and the higher tumor-to-blood ratios [9].

The longer-lived radiometal [89]Zr has emerged as an attractive alternative to [124]I, owing to its residualizing properties *in vivo* [10]. Stillebroer et al. recently reported a preclinical study in mice bearing cRCC tumors directly comparing [89]Zr-cG250 and [124]I-cG250, showing differences in tracer uptake depending on the tumor model [11]. Specifically, these authors observed significantly higher uptake of [89]Zr-cG250 compared with [124]I-cG250 in NU-12 tumors, while there were insignificant differences in uptake between tracers in the SK-RC-52 tumor model. These studies suggest that while residualizing nuclides are generally better suited to the G250/CAIX biology, factors such as: antigen density at the tumor, antigen present within normal tissues such as the gastric mucosa, and prolonged retention of radiometals in liver and spleen, may favor non-residualizing nuclides under some circumstances.

In the current report we compare [124]I-cG250 with [89]Zr-with a non-linear compartmental model to facilitate quantitative comparison of time-dependent uptake and antibody turnover. This model also better relates the imaging data to biologic features of antibody-receptor binding such as internalization of the antibody-antigen complex. The model also supports a preliminary assessment of the potential benefits of radiolabeling cG250 with [89]Zr versus [124]I as a PET tracer for cRCC. We conducted *in vitro* cell binding assays using the human cRCC line SK-RC-38 to determine the kinetics of antigen-antibody binding and evaluate the effect of the radionuclide on the activity of the antibody (e.g. K_d, B_{max}, immunoreactivity). Next, we conducted serial PET imaging and biodistribution experiments to evaluate the fate of each tracer in athymic nude mice bearing sub-cutaneous (s.c.) SK-RC-38 xenografts. Each tracer was evaluated at administered doses of less than 100 μg, expected to be sub-saturating based on the observed *in vitro* B_{max} and occupancy observed (i.e. absolute uptake) during experiments *in vivo*. A description of initial experiments in abstract form was presented at the 2012 World Molecular Imaging Congress, Dublin, Ireland [12].

MATERIALS AND METHODS

Reagents, Antibodies, Cells, and Mice

Unless otherwise noted, all chemicals were obtained from Sigma-Aldrich (Milwaukee, WI) or Fisher Scientific (Pittsburg, PA) and used without further purification. Ultra-pure water (18.2 MΩ·cm) was obtained from an Alpha-Q Ultrapure water system (Millipore). The chimeric monoclonal antibody cG250 and the RCC line SK-RC-38 were supplied by the Ludwig Institute for Cancer Research Center (New York, NY). Cells were grown by serial passage and maintained in RPMI media supplemented with 1% glutamine, 50 units/mL penicillin, 50 units/mL streptomycin, and 10% heat-inactivated fetal bovine serum at 37 °C in a 5% CO_2 environment. Female athymic nude mice (Hsd:Athymic Nude-*Foxn1^{nu}*, 6 – 8 weeks old, 20–25 g) were obtained from Harlan Laboratories (Indianapolis, IN). All antibody injections were performed intravenously (i.v.) via the lateral vein. All animal experiments were approved by the Institutional Animal Care and Use Committee of

Memorial Sloan-Kettering Cancer Center, and institutional guidelines for the proper and humane use of animals in research were followed.

Antibody Conjugation and Radiolabeling

The cG250 antibody was conjugated with isothiocyanatobenzyl-desferrioxamine (SCN-DFO) (Macrocyclics, Dallas, TX) and radiolabeled using methods previously described by Vosjan, *et al.* [13]. ^{89}Zr was provided by the Memorial Sloan-Kettering Radiochemistry & Molecular Imaging Probes Core Facility according to previously reported methods at a specific activities (SA) of 195–497 MBq/μg [14]. The resulting DFO-cG250 bioconjugate showed a DFO-to-antibody mole ratio of 3.25 ± 0.07, as assessed by isotope titration according to the method of Anderson and Meares [15]. Radiolabeling of DFO-cG250 with ^{89}Zr was carried out under neutral buffer conditions and gentle incubation (room temperature for 1 hour (h)) to a final SA of ~360 MBq/mg with radiochemical yields (RCY) 80%. The radiochemical purity (RCP) was determined to be >99% by instant thin-layer chromatography (I-TLC) using 5 mM DTPA, pH 5.0. The stability of ^{89}Zr-cG250 in human serum was evaluated *in vitro* over 11 days (d) at 37 °C by I-TLC, showing that 97.8% of the total ^{89}Zr activity remained in a form consistent with ^{89}Zr-cG250 over the course of the study. ^{124}I was either provided in-house or purchased commercially (IBA Molecular). The RCY of $^{131/124}$I-cG250 ranged from 58–60%, with SA ranging 122–174 MBq/mg and with RCP consistently >99% by I-TLC using 10% trichloroacetic acid (TCA). The *in vivo* stability of ^{124}I-cG250 was evaluated in normal mice (no blocking of thyroid) to determine tracer de-iodination in the absence of tumor. I-TLC analysis with 10% trichloroacetic acid (TCA) of blood up to 3 d post-injection (p.i.) suggested that ^{124}I-cG250 was stable in circulation, as >99% of the total ^{124}I activity was TCA-insoluble, consistent with intact protein (i.e. ^{124}I-cG250). The whole-body activity (WBA) data up to 10 d p.i. were fit to mono-exponential function, yielding a half-life of 52 h ($R^2 = 0.98$). ^{131}I was obtained from Nordion. ^{124}I-cG250 (and, as a surrogate, ^{131}I-cG250) were prepared according to clinical protocols [16, 17]. Activity measurements were made using a CRC-15R Dose Calibrator (Capintec, Ramsey, NJ). Gamma counting was conducted using an automatic well counter (Perkin Elmer Wallac Wizard 3″ Automatic Gamma Counter) calibrated (in terms of counts per minute (min) per kBq, cpm/kBq) for the respective isotopes.

Cell-Binding, Internalization, and Catabolism of Radiolabeled Antibodies

Saturation binding assays were performed as previously described [18, 19] and analyzed using Scatchard analysis and a non-linear regression saturation binding (one-site, specific-binding) method, following subtraction of non-specific binding (Prism, GraphPad Software, Inc.). Immunoreactivity was determining using the Lindmo method [20]. For internalization assays, cells were harvested and added to 12-well plates (500,000 cells/well, 1 mL). After allowing cells to seed overnight, 70 ng of radiolabeled antibody in 10 μL was added to each well (47 pM final concentration) and was incubated at either 37 or 4 °C. At various incubation time points between 15 min and 48 h at 37 °C and between 15 min and 24 h at 4°C ($n = 4$), media was removed and the cells gently washed with ice-cold PBS followed by ice-cold 0.1 M acetic acid + 0.1 M glycine (allowing to incubate for 1 min) and 1 M NaOH (5 min incubation). The activity in all media and washes was assayed by counting in the gamma counter. At 48 h, aliquots of harvested media were assayed by methanol

precipitation to determine the extent of radiolabeled antibody degradation and catabolism following incubation with cells [21].

Mouse RCC Xenograft Models and PET Imaging

Mice were allowed to acclimate for a minimum of 1 week and tumors were induced in the right hind-limb s.c. injection of $5.0 - 10.0$ ($\times 10^6$) cells in a 200 μL cell suspension of a 1:1 (v:v) mixture of media with reconstituted basement membrane (BD Matrigel™, Collaborative Biomedical Products Inc., Bedford, MA). Palpable tumors were observed in 6–8 weeks.

For PET imaging studies, mice bearing s.c. SK-RC-38 xenografts were injected i.v. with ^{89}Zr-cG250 (14.6–15.0 MBq, 40 μg, 267 pmol) or ^{124}I-cG250 (11.8–12.6 MBq, 100 μg, 667 pmol) in 200 μL of saline + 1% BSA. At various time points p.i. ranging from 5–264 h for ^{89}Zr and from 7–240 h for ^{124}I, mice were scanned using a microPET Focus 120 (Concorde Microsystems, Knoxville, TN) while under anesthesia using a mixture of 1.5–2% isofluorane (Baxter Healthcare, Deerfield, IL) and air. In addition, animals were assayed for WBA in the dose calibrator at each imaging time point as described above. Imaging data were acquired using an energy window of 350–700 keV and a coincidence timing window of 6 ns; the scan times were adjusted to acquire a minimum of 20 million coincidence events up to a maximum of 1 h beyond 7 d p.i.. Data were sorted into 2-dimensional histograms by Fourier rebinning, and image reconstruction was performed by filtered backprojection with a $128 \times 128 \times 6$ matrix ($0.72 \times 0.72 \times 1.33$ mm). The resulting images were parameterized (as %ID/g) by first converting the voxel-counting rates to activity concentrations using empirically determined calibration factors for each isotope, followed by decay-correction to the time of injection and normalization to the administered activity. Two-dimensional regions of interest (ROI) were manually drawn for tumor and blood pool (the heart region) using ASIPro VM™ software (Concorde Microsystems). Tumor ROI values were corrected for partial-volume effect using phantom-derived volume-dependent recovery coefficients and calculated tumor volumes (V), calculated as $V = (\pi/6)d^3$ where d is the caliper-measured tumor diameter.

Biodistribution

After the final PET aquisition, mice were euthanized by CO_2 (g) asphyxiation for *ex vivo* biodistribution studies. Three mice previously injected with ^{124}I-cG250 were sacrificed at 168 h p.i. due to the WBA observed to be less than 0.37 MBq. For comprehensive serial biodistribution studies of ^{89}Zr-cG250, 1.85 MBq (5 μg) in 200 μL of saline + 1% BSA were injected via the tail vein into mice bearing s.c. SK-RC-38 tumors. Count data were background- and decay-corrected to the time of injection and then converted to activity using the isotope-specific calibration factor. Uptake for each tissue sample was calculated by normalization to the total activity injected and expressed as percent injected dose per gram (%ID/g).

Statistical Analysis

Differences in tissue uptake between cohorts were analyzed for statistical significance by the Student's *t* test for paired data. Two-sided significance levels were calculated and $p<0.05$ was considered statistically significant.

Compartmental Modeling

The [124]I- and [89]Zr-cG250 mean tumor ROI concentration data in the tumor-bearing mice were fit to the nonlinear compartmental model shown in Figure 1 using the SAAM II (Simulation, Analysis, and Modeling) computer program. The measured plasma time-activity data provide the direct input function for tumor, eliminating the need to explicitly account for the antibody in the rest of the body (*i.e.* in tissues other than tumor). For fitting, the starting values of the association rate constant (k_a) and the antigen (ie CAIX) concentration in tumor ($[Ag]_{tumor}$) were measured *in vitro* as described in the previous sections. All model parameters were then adjusted to yield the best fit of the model-predicted to the measured tumor time-activity concentration data. Implicit in the model shown in Figure 1 is the assumption that there is no significant dissociation of the bound cG250 from CAIX (as indicated by the absence of the k(2,0) exchange rate in the model). Note that the parameter k(2,1) equals = k_a $[Ab]_{plasma}$ {Total $[Ag]_{tumor}$ − $[AbAg]_{tumor}$}; the second term (*i.e.* the difference term) makes the k(2,1) time-varying parameters and thus introduces a non-linearity into the model.

RESULTS

In vitro characterization of radiolabeled cG250

For all radiolabeled antibodies, the immunoreactivity was observed to be >90% using the Lindmo assay. Scatchard analysis of binding capacity (*Bmax*) of [89]Zr-cG250 and [131/124]I-cG250 to SK-RC-38 yielded $218,000 \pm 5600$ and $167,000 \pm 3900$ antibody molecules bound per cell, respectively. This corresponds to approximately 280–450 pmol/g tumor *in vivo* (assuming 10^9 cells per g of tumor [17]). The affinity of each tracer (K_d) was also determined to be 5.33 ± 0.52 nM and 1.51 ± 0.08 nM for [89]Zr-, and ^{131}I-labeled cG250, respectively.

The kinetics of radiolabeled antibody internalization by cRCC cells was studied by incubating the radiotracer with cells seeded in 12-well plates. [89]Zr- and [131]I- were observed to be present on the cell-surface at tracer concentrations of 3% and 1% of the total added activity after 24 h, respectively, and remain unchanged at 48 h (Figure 2). Internalization data obtained up to 48 h were fit to a mono-exponential function, and the bound-antibody internalization rate was determined to be 20% per hour for both radiolabeled forms of the antibody. At 48 h, the percent of activity in harvested media that was methanol-precipitable for [89]Zr-cG250 and ^{131}I-cG250 was $73.7 \pm 3.1\%$ and $56.4 \pm 0.7\%$, respectively ($p < 0.005$).

Noninvasive serial PET imaging and tumor uptake measurement

Small-animal PET studies with [89]Zr-cG250 and [124]I-cG250 were performed in athymic nude mice bearing SK-RC-38 xenografts, with imaging at various time points from 5 h to 11 d p.i.. Figure 3 shows a representative time series of PET images obtained with each tracer.

The serial PET studies showed that both [124]I- and [89]Zr-cG250 can lead to high-contrast imaging of a subcutaneous model of cRCC *in vivo*, but with notable differences in tumor uptake and retention of the tracer. Tumor activity concentrations were expressed as the maximum %ID/g in manually drawn two-dimensional tumor-contouring ROIs (Figure 4). At 5 h p.i., the activity concentration of both the [124]I and [89]Zr radiolabels were sufficiently high relative to background to produce high-contrast tumor images (due, in part, to the location of the xenograft in the flank and the absence of significant contiguous background activity), but contrast was improved at 24 h p.i.. Uptake of [89]Zr-cG250 increased over 48 h p.i. to a plateau of ~20 %ID/g, which persisted to the last imaging time point at 11 d p.i.. With [124]I-cG250, a peak uptake of ~5 %ID/g was observed at 5–24 h p.i., with subsequent washout to ~2 %ID/g at 10 d p.i.. Time-activity curves for thyroid uptake of [124]I are provided in Supplemental Information, S1

The whole-body clearance kinetics of each tracer was determined in tumor-bearing mice. The effective *in vivo* half-lives were 55 h ($R^2 = 0.90$) for [89]Zr and 43 h ($R^2 = 0.75$) and 35 h ($R^2 = 0.87$), for [124]I without and with thyroid blocking, respectively. In addition, biodistribution studies of both [124]I-cG250 and [89]Zr-cG250 groups and were conducted (10 d and 11 d p.i., respectively) (Figure 5 and Supplemental Information, S2). The concentrations of tracer in tissue measured by well counting agreed closely with the PET-derived data with the exception of the tumor, with similar activity in blood-rich tissues (heart, lungs), and significantly different tumor activities (40 %ID/g and 5 %ID/g for [89]Zr and [124]I, respectively). Incomplete correction for partial-volume effect for small tumors probably explains the differences between PET- and well-counter-derived activity concentrations. Higher concentrations of [89]Zr-cG250 than [124]I-cG250 were found in liver ($p < 0.05$), spleen, kidney, and bone (all $p < 0.005$), presumably due to the metabolism of radiometal complexes *in vivo* and the affinity of bone for free [89]Zr [22]. Such non-specific tracer uptake in normal tissue, especially in the liver and bone, are of particular concern for pre-surgical diagnosis of advanced metastatic disease, as well as dosimetry planning for RIT [23].

Results of the non-linear compartmental modeling of [89]Zr-cG250 and [124]I-cG250 in the tumor-bearing mice are shown graphically in Figure 6. The "best-fit" model parameters were as follows: for [89]Zr-cG250, $k_a = 3.5 \times 10^{10}$ h^{-1}M^{-1}, total [Ag]$_{tumor}$ = 3.1 μM, k(0,3) = 8.33×10^{-4} h^{-1}, and k(3,2) = 0.20 h^{-1}; for [124]I-cG250, $k_a = 8.0 \times 10^{9}$ h^{-1}M^{-1}, total [Ag]$_{tumor}$ = 3.1 μM, k(0,3) = 1.46×10^{-2} h^{-1}, and k(3,2) = 0.20 h^{-1}. The 17.5-fold higher value of k(0,3) for [124]I- than for [89]Zr-cG250 is particularly notable, as it reflects the rapid washout of the non-residualizing [124]I from the tumor compared to the stable tumor activity of the residualizing [89]Zr in the tumor. Based on the foregoing model parameters, quasi-equilibrium activity concentrations in tumor, and the administered dose of antibody (in moles), one can calculate that 5.52×10^{12} molecules of bound [89]Zr-cG250 are internalized per hour per gram of tumor and 4.60×10^{9} atoms of [89]Zr (or only about 0.08% of those internalized) are released per hour per gram of tumor. Conversely, 1.35×10^{12} molecules of bound [124]I-cG250 are internalized per hour per gram of tumor and 1.97×10^{10} atoms of [124]I (or about 1.46% of those internalized) are released per hour per gram of tumor.

DISCUSSION

Our aim was to model the relationship between antibody-antigen binding and internalization properties by using quantitative non-invasive PET imaging with two distinct radiotracers in a single pre-clinical mouse xenograft model of cRCC. It has been previously documented that conjugating cG250 with a residualizing radiotracer will give higher-contrast imaging of RCC tumors in mice. [24]. We reasoned that a more comprehensive pair-wise comparison of [89]Zr- and [124]I-cG250 both *in vitro* and *in vivo* would allow for the development of a kinetic model that could take into account (1) the specific of tracers *in vitro* and (2) the rate of degradation and extent of release of tracer metabolites from the cell. We believe this approach leads to a more accurate estimation of the residence time and antibody-antigen turnover kinetics in tumor *in vivo*. We began our study with an evaluation of the *in vitro* disposition of the two tracers using the human RCC cell line SK-RC-38. Both [89]Zr- and [124]I-cG250 had binding properties derived from saturation binding studies that were within the same range (5.33 ± 0.52 nM and 1.51 ± 0.08 nM, respectively), as are the number of binding sites per cell ($218,000 \pm 5600$ and $167,000 \pm 3900$, respectively). These apparent differences can be explained by the variability typically encountered in such biological assays. Next, a continuous uptake assay was performed to determine the kinetics of surface binding and subsequent internalization. We observed that the internalized fraction of both [89]Zr- and [124]I-cG250 gradually increased at the same rate (20% per hour), until a maximum of 60–70% of total added activity was reached at 24 h, which remained unchanged at 48 h. In addition, a very small fraction of membrane bound activity (< 5%, up to 48 h) was isolated using a low-pH wash at all time points. These data suggest that both radioantibody forms are rapidly internalized and accumulate in the cell, ultimately trafficking to the lysosome, where the antigen-antibody complexes are catabolized [25]. To further characterize the antibody-antigen turnover *in vitro*, aliquots of the cellular supernatants were subjected to methanol precipitation after incubation for 48 h at 37°C. Compared with [89]Zr, a greater abundance of iodine metabolites appeared in the extra-cellular media (~50% of total activity was methanol-insoluble/protein-associated at 48 h). These observations are consistent with previous *in vitro* studies of radiolabeled G250 stability [26] as well as G250/CAIX internalization and tracer fate using human RCC lines [17]. The identical serum stability of the tracers indicated little change in the status of the radiometal antibody but a decrease in the radioiodinated fraction of antibody, consistent with the concept that it was low-MW forms of radioiodine which were released from the cells.

Mice bearing RCC-xenografts were administered [89]Zr- or [124]I-cG250 and serially imaged by PET over the course of 10–11 d p.i. to determine the kinetics of tracer uptake in the tumor and rates of clearance from the vascular compartment. While both tracers allowed for high-contrast imaging of RCC, the comparative intra-tumoral concentrations varied significantly from 5 h–10 d p.i.. This observation could not be explained by differences in clearance, as the biological half-lives as determined by quantitation of activity in circulation were not significantly different. The washout of [124]I-tracer from the tumor due to RCC catabolism was supported by the observation of radioiodine accumulation in the thyroid observed during PET imaging as well as more rapid whole-body clearance.

In developing antibody-based therapies such as cytotoxic drug or radioimmunoconjugates, quantitatively characterizing the biology of the antibody-antigen interaction, internalization, and turnover is valuable [27]. Many groups have described kinetic models that provide insight into the relationship between the *in vitro* and *in vivo* behavior of antibodies [28–30]. By evaluating a particular antibody candidate using both residualizing and non-residualizing radioactive labels (e.g. serial imaging with PET to non-invasively quantify tracer in tissue), the turnover kinetics can be determined and applied to a kinetic model that can estimate the residence time of a particular label as a function of dose. With efforts increasing to engineer antibodies that offer improved affinity, immunomodulatory response, or with desirable internalization kinetics (e.g. for CAIX [31]), the use of a kinetic model can guide selection of an optimum antibody construct for a particular patient and application as well as of optimum patient-specific doses (in terms of moles). This can be applied not only to radiolabeled antibody forms but toxin- or drug-conjugated antibody constructs. If a residualizing radiolabel such as ^{89}Zr were incorporated into such a therapeutic antibody-drug construct, the tumor area under the curve (AUC) for the radiolabel would serve as a surrogate metric of the drug AUC and thus could be used to plan and optimize antibody-mediated drug therapy. In addition, insight into the effects of refining targeting strategies such as modulating intracellular delivery and traffic dynamics (e.g. with conjugation of membrane-destabilizing synthetic polymers such as poly(propylacrylic acid [32]) or antigen accessibility (e.g. with microtubule depolymerizing drugs in the case of PSMA-targeting [33]) can potentially be evaluated.

According to our studies, ^{89}Zr- and ^{124}I-cG250 demonstrate virtually identical binding and initial uptake, but the label is metabolized by the cell and differentially released into the media or vascular compartment. *In vivo* kinetic models yielded estimates of internalization of the receptor-bound antibody of 20 %ID/g/h, with minimal release of ^{89}Zr but with comparable uptake of ^{124}I-cG250 leading to release of considerable amounts of ^{124}I. This information can be used to estimate CAIX/cG250 receptor turnover and cG250-accessible antigen density in clinical studies.

The development of this kinetic model was based on our prior studies of immunoPET in humans, wherein it was discovered that in vivo the antigen targeting of antibody was driven by the law of mass action [34]. The modeling of this process requires saturable and therefore non-linear kinetics, dependent on the concentrations of free reactants and the antibody-antigen affinity. The resulting model (Figure 1) can accommodate the biology of internalization of the antibody-antigen complex. In essence, the rate of uptake of the radiotracer, retention, and release can ultimately be determined from a non-invasive quantitative imaging assay such as PET.

CONCLUSION

By comparing the differential catabolism of the two radioantibody forms, ^{124}I cG250, and ^{89}Zr-cG250, we determined the relationship between the biology of the cG250/CAIX interaction and subsequent processes (internalization and catabolism). The distinct radioantibody formulations were virtually identical in terms of clearance from the blood, initial tumor binding and uptake, and rate of internalization of the cG250-CAIX antibody

receptor complex. However, there were marked differences in the rate of clearance from tumor, with the [124]I atoms being cleared from tumor more than 17.5 times more rapidly than [89]Zr – the presumed basis of the longer tumor retention for the pronounced advantage in tumor imaging of the [89]Zr-labeled antibody over [124]I-labeled antibody for cG250/CAIX.

Supplementary Material

Refer to Web version on PubMed Central for supplementary material.

Acknowledgments

References

1. Divgi CR, Pandit-Taskar N, Jungbluth AA, Reuter VE, Gonen M, Ruan S, et al. Preoperative characterisation of clear-cell renal carcinoma using iodine-124-labelled antibody chimeric G250 (124I-cG250) and PET in patients with renal masses: a phase I trial. Lancet Oncol. 2007; 8:304–10. [PubMed: 17395103]

2. Divgi CR, Uzzo RG, Gatsonis C, Bartz R, Treutner S, Yu JQ, et al. Positron emission tomography/ computed tomography identification of clear cell renal cell carcinoma: results from the REDECT trial. J Clin Oncol. 2013; 31:187–94. [PubMed: 23213092]

3. Rice SL, Roney CA, Daumar P, Lewis JS. The next generation of positron emission tomography radiopharmaceuticals in oncology. Semin in Nucl Med. 2011; 41:265–82. [PubMed: 21624561]

4. Oosterwijk E, Ruiter DJ, Hoedemaeker PJ, Pauwels EK, Jonas U, Zwartendijk J, et al. Monoclonal antibody G 250 recognizes a determinant present in renal-cell carcinoma and absent from normal kidney. Int J of Cancer. 1986; 38:489–94. [PubMed: 2428759]

5. Perk LR, Vosjan MJ, Visser GW, Budde M, Jurek P, Kiefer GE, et al. p-Isothiocyanatobenzyl-desferrioxamine: a new bifunctional chelate for facile radiolabeling of monoclonal antibodies with zirconium-89 for immuno-PET imaging. Eur J Nucl Med Mol Imaging. 2010; 37:250–9. [PubMed: 19763566]

6. Stillebroer AB, Boerman OC, Desar IM, Boers-Sonderen MJ, van Herpen CM, Langenhuijsen JF, et al. Phase 1 Radioimmunotherapy Study with Lutetium 177-labeled Anti-Carbonic Anhydrase IX Monoclonal Antibody Girentuximab in Patients with Advanced Renal Cell Carcinoma. Eur Urol. 2013; 64:478–85. [PubMed: 22980441]

7. Press OW, DeSantes K, Anderson SK, Geissler F. Inhibition of catabolism of radiolabeled antibodies by tumor cells using lysosomotropic amines and carboxylic ionophores. Cancer Res. 1990; 50:1243–50. [PubMed: 2297772]

8. Press OW, Shan D, Howell-Clark J, Eary J, Appelbaum FR, Matthews D, et al. Comparative metabolism and retention of iodine-125, yttrium-90, and indium-111 radioimmunoconjugates by cancer cells. Cancer Res. 1996; 56:2123–9. [PubMed: 8616860]

9. Brouwers AH, Buijs WC, Oosterwijk E, Boerman OC, Mala C, De Mulder PH, et al. Targeting of metastatic renal cell carcinoma with the chimeric monoclonal antibody G250 labeled with (131)I or (111)In: an intrapatient comparison. Clin Cancer Res. 2003; 9:3953S–60S. [PubMed: 14506194]

10. Verel I, Visser GW, Boellaard R, Boerman OC, van Eerd J, Snow GB, et al. Quantitative 89Zr immuno-PET for in vivo scouting of 90Y-labeled monoclonal antibodies in xenograft-bearing nude mice. J Nucl Med. 2003; 44:1663–70. [PubMed: 14530484]

11. Stillebroer AB, Franssen GM, Mulders PF, Oyen WJ, van Dongen GA, Laverman P, et al. ImmunoPET Imaging of Renal Cell Carcinoma with (124)I- and (89)Zr-Labeled Anti-CAIX Monoclonal Antibody cG250 in Mice. Cancer Biother Radiopharm. 2013; 28:510–5. [PubMed: 23697926]

12. Cheal, SM.; Punzalan, B.; Doran, M.; Evans, MJ.; Zanzonico, P.; Lewis, JS., et al. Pairwise PET Imaging Comparisons of 89Zr and 124I labeled cG250 as a Basis for Non-Invasive Quantitation of In Vivo CAIX Receptor Binding and Internalization in Mouse Xenografts of Clear Cell Renal Carcinoma. Molecular Imaging and Biology; Proceedings of the 2012 World Molecular Imaging Congress; Dublin, Ireland. September 5–8, 2012 December 2012; 2012.

13. Vosjan MJ, Perk LR, Visser GW, Budde M, Jurek P, Kiefer GE, et al. Conjugation and radiolabeling of monoclonal antibodies with zirconium-89 for PET imaging using the bifunctional chelate p-isothiocyanatobenzyl-desferrioxamine. Nature Protoc. 2010; 5:739–43. [PubMed: 20360768]

14. Holland JP, Sheh Y, Lewis JS. Standardized methods for the production of high specific-activity zirconium-89. Nucl Med and Biol. 2009; 36:729–39. [PubMed: 19720285]

15. Anderson CJ, Schwarz SW, Connett JM, Cutler PD, Guo LW, Germain CJ, et al. Preparation, biodistribution and dosimetry of copper-64-labeled anti-colorectal carcinoma monoclonal antibody fragments 1A3-F(ab′)2. J Nucl Med. 1995; 36:850–8. [PubMed: 7738663]

16. Divgi CR, Bander NH, Scott AM, O'Donoghue JA, Sgouros G, Welt S, et al. Phase I/II radioimmunotherapy trial with iodine-131-labeled monoclonal antibody G250 in metastatic renal cell cancer. Clin Cancer Res. 1998; 4:2729–39. [PubMed: 9829736]

17. Kranenborg MH, Boerman OC, de Weijert MC, Oosterwijk-Wakka JC, Corstens FH, Oosterwijk E. The effect of antibody protein dose of anti-renal cell carcinoma monoclonal antibodies in nude mice with renal cell carcinoma xenografts. Cancer. 1997; 80:2390–7. [PubMed: 9406688]

18. Carlin S, Khan N, Ku T, Longo VA, Larson SM, Smith-Jones PM. Molecular targeting of carbonic anhydrase IX in mice with hypoxic HT29 colorectal tumor xenografts. PloS one. 2010; 5:e10857. [PubMed: 20523727]

19. Smith-Jones PM, Vallabahajosula S, Goldsmith SJ, Navarro V, Hunter CJ, Bastidas D, et al. In vitro characterization of radiolabeled monoclonal antibodies specific for the extracellular domain of prostate-specific membrane antigen. Cancer Res. 2000; 60:5237–43. [PubMed: 11016653]

20. Lindmo T, Boven E, Cuttitta F, Fedorko J, Bunn PA Jr. Determination of the immunoreactive fraction of radiolabeled monoclonal antibodies by linear extrapolation to binding at infinite antigen excess. J Immunol Methods. 1984; 72:77–89. [PubMed: 6086763]

21. Yao Z, Garmestani K, Wong KJ, Park LS, Dadachova E, Yordanov A, et al. Comparative cellular catabolism and retention of astatine-, bismuth-, and lead-radiolabeled internalizing monoclonal antibody. Journal of nuclear medicine: official publication, Society of Nuclear Medicine. 2001; 42:1538–44.

22. Abou DS, Ku T, Smith-Jones PM. In vivo biodistribution and accumulation of 89Zr in mice. Nuclear medicine and biology. 2011; 38:675–81. [PubMed: 21718943]

23. Lam JS, Leppert JT, Belldegrun AS, Figlin RA. Adjuvant therapy of renal cell carcinoma: patient selection and therapeutic options. BJU Int. 2005; 96:483–8. [PubMed: 16104896]

24. Brouwers A, Verel I, Van Eerd J, Visser G, Steffens M, Oosterwijk E, et al. PET radioimmunoscintigraphy of renal cell cancer using 89Zr-labeled cG250 monoclonal antibody in nude rats. Cancer Biother Radiopharm. 2004; 19:155–63. [PubMed: 15186595]

25. Geissler F, Anderson SK, Venkatesan P, Press O. Intracellular catabolism of radiolabeled anti-mu antibodies by malignant B-cells. Cancer Res. 1992; 52:2907–15. [PubMed: 1581908]

26. Brouwers AH, van Eerd JE, Frielink C, Oosterwijk E, Oyen WJ, Corstens FH, et al. Optimization of radioimmunotherapy of renal cell carcinoma: labeling of monoclonal antibody cG250 with 131I, 90Y, 177Lu, or 186Re. J Nucl Med. 2004; 45:327–37. [PubMed: 14960657]

27. Ritchie M, Tchistiakova L, Scott N. Implications of receptor-mediated endocytosis and intracellular trafficking dynamics in the development of antibody drug conjugates. mAbs. 2013; 5:13–21. [PubMed: 23221464]

28. Mano Y, Suzuki H, Terasaki T, Iwahashi T, Ono K, Naito M, et al. Kinetic analysis of the disposition of MRK16, an anti-P-glycoprotein monoclonal antibody, in tumors: comparison between in vitro and in vivo disposition. J Pharm Exper Ther. 1997; 283:391–401.

29. Thurber GM, Weissleder R. Quantitating antibody uptake in vivo: conditional dependence on antigen expression levels. Mol Imaging Biol. 2011; 13:623–32. [PubMed: 20809210]

30. Rao BM, Lauffenburger DA, Wittrup KD. Integrating cell-level kinetic modeling into the design of engineered protein therapeutics. Nature Biotech. 2005; 23:191–4.

31. Xu C, Lo A, Yammanuru A, Tallarico AS, Brady K, Murakami A, et al. Unique biological properties of catalytic domain directed human anti-CAIX antibodies discovered through phage-display technology. PloS one. 2010; 5:e9625. [PubMed: 20224781]

32. Berguig GY, Convertine AJ, Shi J, Palanca-Wessels MC, Duvall CL, Pun SH, et al. Intracellular Delivery and Trafficking Dynamics of a Lymphoma-Targeting Antibody-Polymer Conjugate. Mol Pharm. 2012; 9:3506–3514. [PubMed: 23075320]

33. Christiansen JJ, Weimbs T, Bander N, Rajasekaran AK. Differing effects of microtubule depolymerizing and stabilizing chemotherapeutic agents on t-SNARE-mediated apical targeting of prostate-specific membrane antigen. Mol Cancer Ther. 2006; 5:2468–73. [PubMed: 17041090]

34. O'Donoghue JA, Smith-Jones PM, Humm JL, Ruan S, Pryma DA, Jungbluth AA, et al. 124I-huA33 antibody uptake is driven by A33 antigen concentration in tissues from colorectal cancer patients imaged by immuno-PET. J Nucl Med. 2011; 52:1878–85. [PubMed: 22068895]
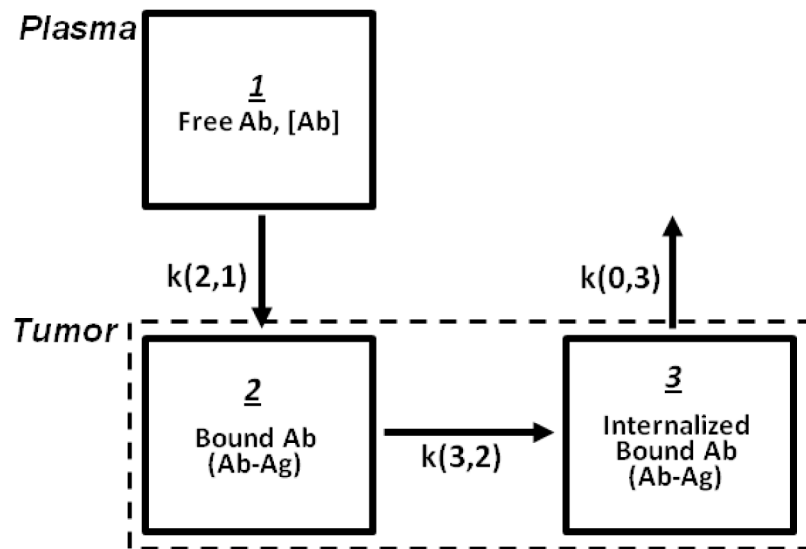
FIGURE 1.
Non-linear compartmental model of intravenously injected radiolabeled cG250 antibody in mice with the CAIX-expressing tumor xenografts. The parameter k(i,j) is the fractional rate (/h) of exchange of the radiolabel from compartment j to compartment i.
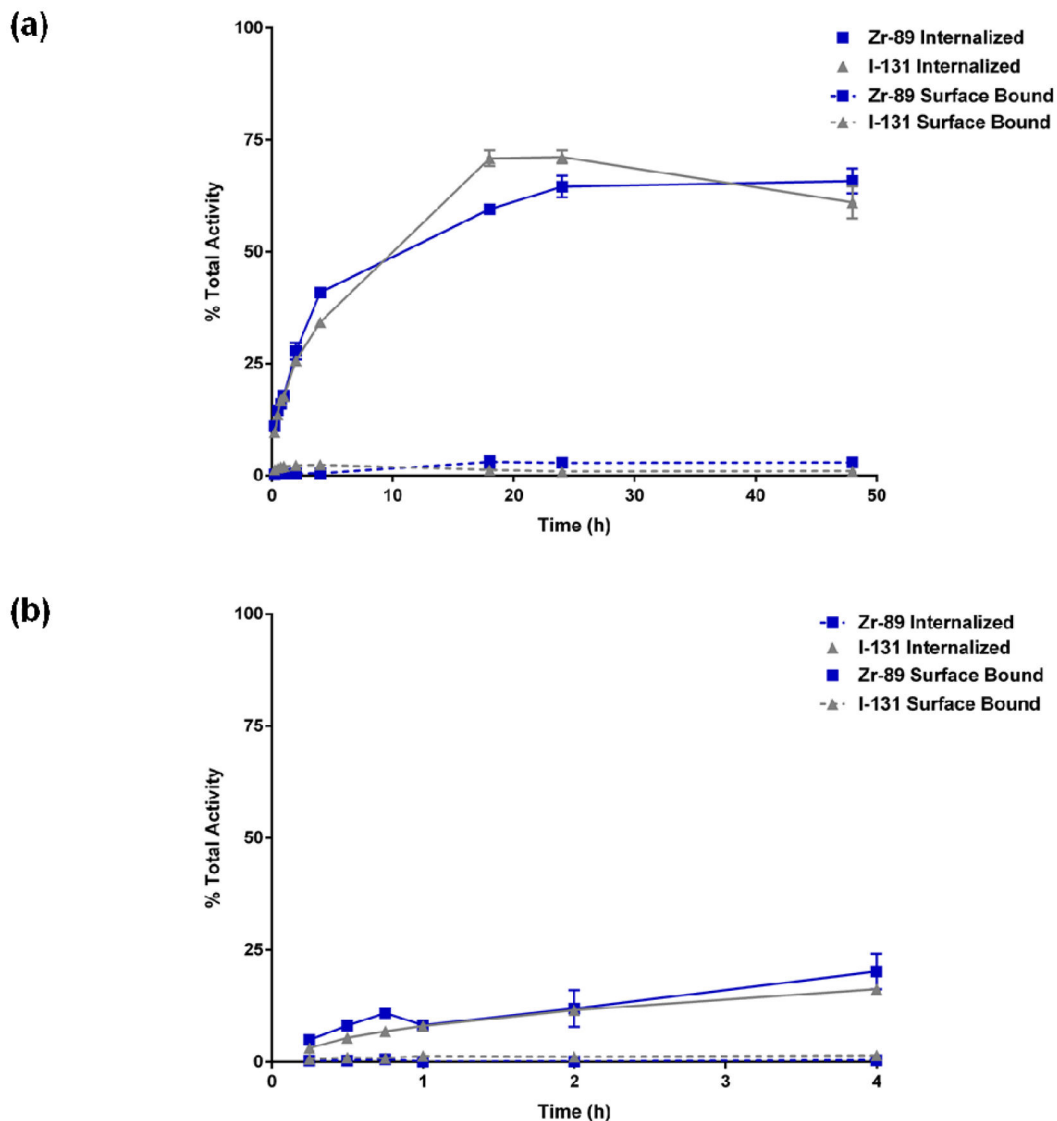
FIGURE 2.
Analysis of internalization and cell-surface binding at 37°C up to 48 h (*top graph* (**a**)) and 4°C up to 4 h (*bottom graph* (**b**)) in vitro of ^{89}Zr-cG250 and ^{131}I-cG250 by the RCC cell line SK-RC-38.
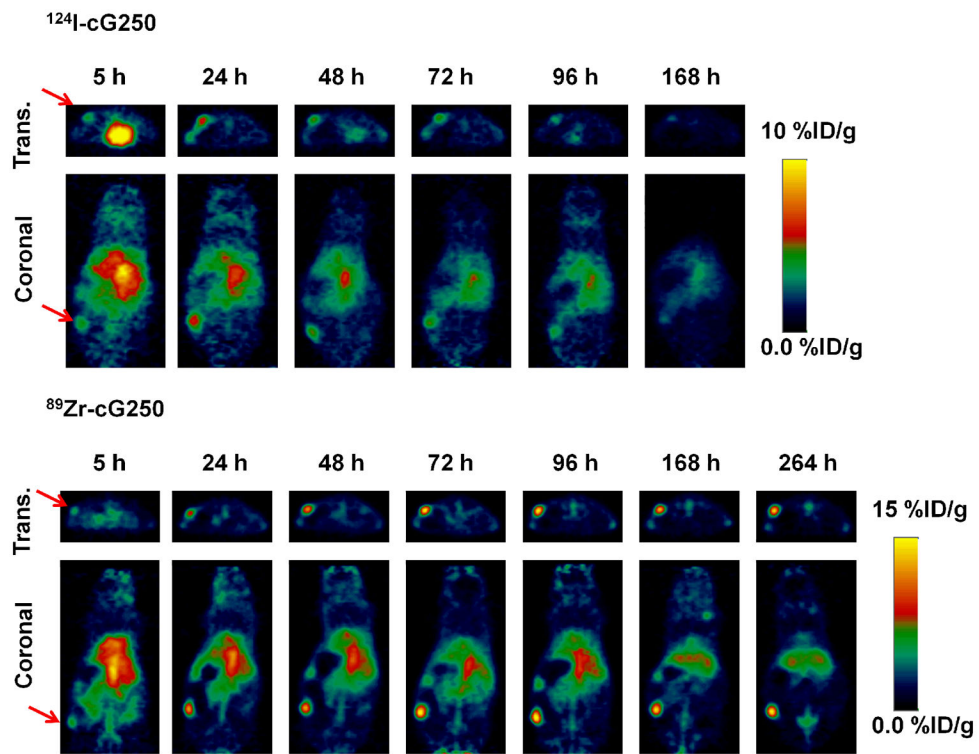
FIGURE 3.
Noninvasive serial-PET imaging in tumor-bearing mice. Representative transverse (trans.) and coronal PET images of nude mice bearing subcutaneous SK-RC-38 xenografts in the lower hind limb imaged with [124]I- or [89]Zr-cG250 at various time points up to 11 d p.i.. Arrows indicate position of tumor. Images are parameterized as %ID/g.
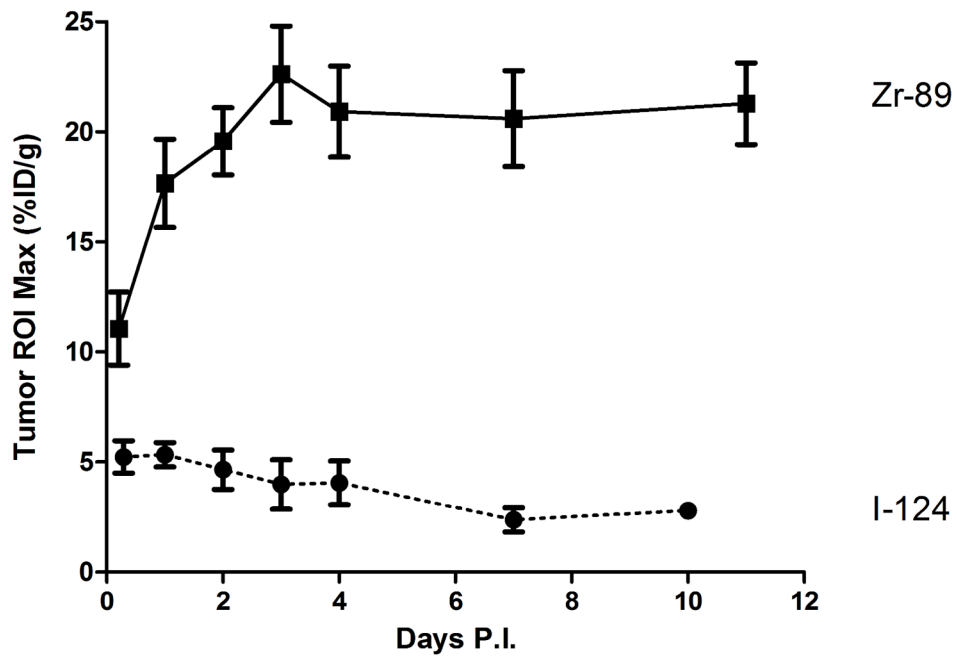
FIGURE 4.
Tumor time-activity ROI concentration curves for [124]I- or [89]Zr-cG250 uptake in SK-RC-38 xenografts (*n* = 5 for each cohort) up to 10 and 11 d p.i., respectively. Data are expressed as (mean ± standard error of the mean (SEM)).
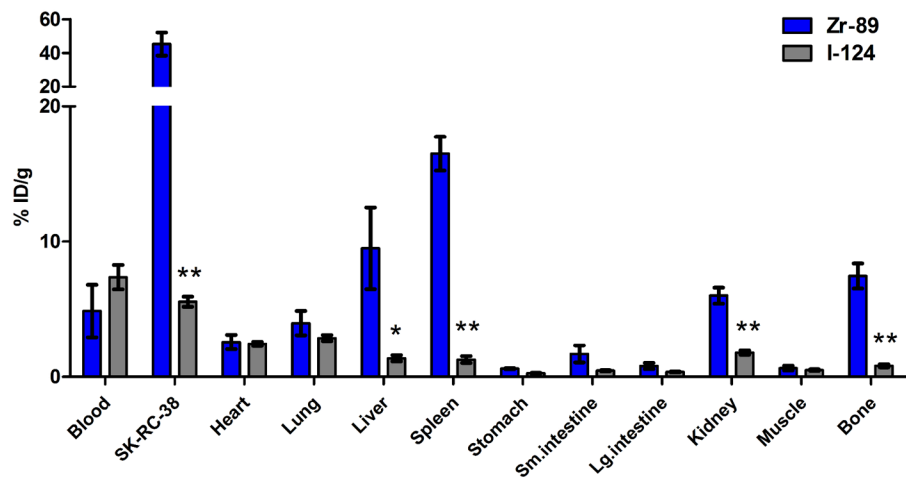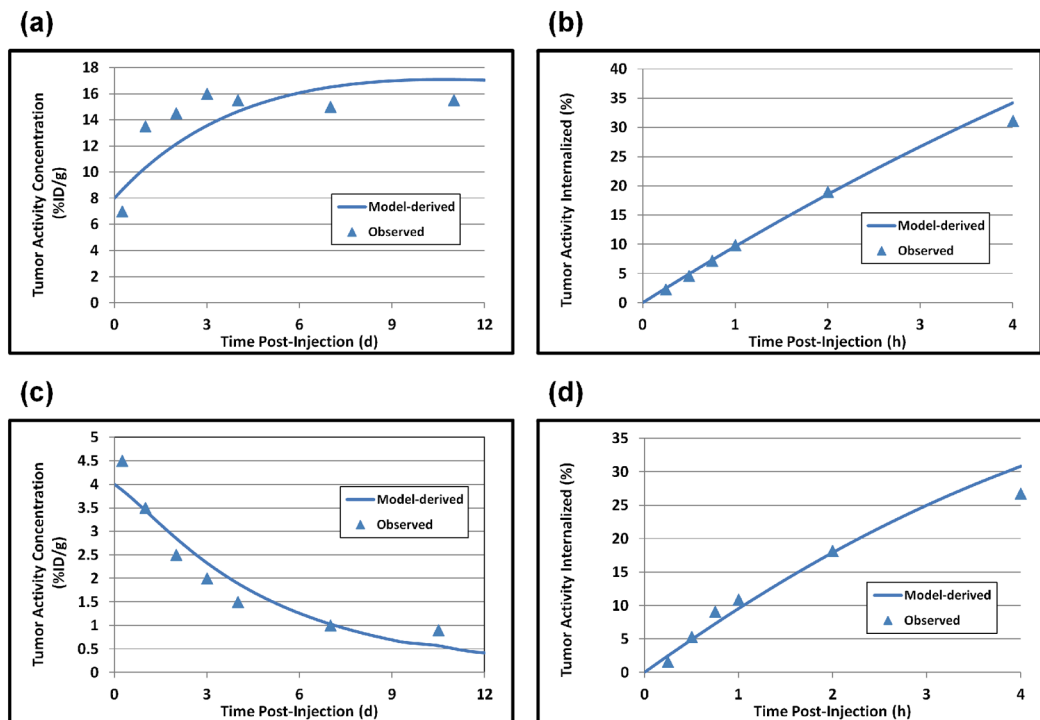
FIGURE 5.
Biodistribution data following serial PET imaging (11 d for ^{89}Zr-cG250 and 10 d for ^{124}I-cG250). Groups consisted of 4 or 5 mice each. Data for ^{124}I-cG250 is from group of animals with normal thyroid at time of tracer injection. The data are expressed as the mean %ID/g $\pm$ SEM. (*) $p < 0.05$, (**) $p < 0.005$.

FIGURE 6.

Results of non-linear compartmental model of intravenously injected radiolabeled cG250 antibody in mice with the CAIX-expressing tumor xenografts. The data points represent the mean values among the mice injected with ^{89}Zr-cG250 ((a) and (b)) and ^{124}I-cG250 ((c) and (d)). Panels (a) and (b) show the observed and model-derived activity concentrations (%ID/g) in tumor and panels (c) and (d) the observed and model-derived activity (% of total tumor activity internalized in the tumor cells). In all cases, the model yields reasonably good fits to the data.